Three-point bending setup for piezoresistive gauge factor measurement of thin-film samples at high temperatures

Dam Madsen, Nis; Kjelstrup-Hansen, Jakob

Published in:
Review of Scientific Instruments

DOI:
10.1063/1.4973512

Publication date:
2017

Document version
Publisher's PDF, also known as Version of record

Citation for pulished version (APA):
Dam Madsen, N., & Kjelstrup-Hansen, J. (2017). Three-point bending setup for piezoresistive gauge factor measurement of thin-film samples at high temperatures. Review of Scientific Instruments, 88(015001). DOI: 10.1063/1.4973512

Three-point bending setup for piezoresistive gauge factor measurement of thin-film samples at high temperatures

Nis Dam Madsen, and Jakob Kjelstrup-Hansen

Citation: Review of Scientific Instruments **88**, 015001 (2017); doi: 10.1063/1.4973512
View online: http://dx.doi.org/10.1063/1.4973512
View Table of Contents: http://aip.scitation.org/toc/rsi/88/1
Published by the American Institute of Physics

Three-point bending setup for piezoresistive gauge factor measurement of thin-film samples at high temperatures

Nis Dam Madsen[a] and Jakob Kjelstrup-Hansen[b]
NanoSYD, Mads Clausen Institute, University of Southern Denmark, Alsion 2, 6400 Sønderborg, Denmark

(Received 8 November 2016; accepted 19 December 2016; published online 4 January 2017)

We present a new method for measuring the piezoresistive gauge factor of a thin-film resistor based on three-point bending. A ceramic fixture has been designed and manufactured to fit a state-of-the-art mechanical testing apparatus (TA Instruments Q800). The method has been developed to test thin-film samples deposited on silicon substrates with an insulating layer of SiO_2. The electrical connections to the resistor are achieved through contacts in the support points. This insures that the influence of the electrical contacts is reduced to a minimum and eliminates wire-bonding or connectors attached to the sample. During measurement, both force and deflection of the sample are recorded simultaneously with the electrical data. The data analysis extracts a precise measurement of the sample thickness (<1% error) in addition to the gauge factor and the temperature coefficient of resistivity. The sample thickness is a critical parameter for an accurate calculation of the strain in the thin-film resistor. This method provides a faster sample evaluation by eliminating an additional sample thickness measurement or alternatively an option for cross checking data. Furthermore, the method implements a full compensation of thermoelectrical effects, which could otherwise lead to significant errors at high temperature. We also discuss the magnitude of the error sources in the setup. The performance of the setup is demonstrated using a titanium nitride thin-film, which is tested up to 400 °C revealing the gauge factor behavior in this temperature span and the temperature coefficient of resistivity. *Published by AIP Publishing.* [http://dx.doi.org/10.1063/1.4973512]

I. INTRODUCTION

Piezoresistive devices are widely used in industry for the control and optimization of processes. The two most common examples of devices exploiting piezoresistivity are pressure sensors and load cells. In recent years, the demand for robust devices, which sustain harsh environments, has been increasing. Many applications, such as engine monitoring, require operating temperatures of up to 400 °C. Devices for such high temperature applications are typically based on thin-film strain sensors deposited using PVD or CVD techniques.[1,2] The development of new thin-film materials typically requires many tests to optimize the material system under investigation. Therefore, accurate and fast testing of samples is desirable.

In the present work, the objective has been to create a test platform which allows accurate measurements up to at least 400 °C. Electro-mechanical characterization at these temperatures is challenging due to the high demands on the materials used for the measurement setup. Another requirement has been that samples fabricated from silicon wafers can be evaluated with a minimum of sample preparation.

Three-point bending was chosen as the straining method because it is gentle to the samples and without uncontrolled strains which can arise in clamped setups. Furthermore, the mounting of samples is straightforward and fast.

However, one particular challenge in the design process was the electrical contacts to the sample. Standard electrical connectors such as FFC (flexible flat cable) connectors cannot be used at these temperatures. Another option is wire bonding, however, bonded wires are delicate and handling is tedious. Furthermore, these connector types may influence the straining of the sample. This problem was overcome by placing contacts in the support points of the fixture. This solution was also suggested by Richter to resolve the above mentioned problems.[3]

Beam bending has previously been used successfully to investigate piezoresistivity by Lund[4] and Richter.[5] In both these setups, four-point bending was used. Four-point bending has the advantage of a constant strain between the inner load points. However, as three-point bending offers two other distinct advantages over four-point bending, we have chosen this approach. First, the deflection of the sample at the load point(s) is larger in three-point than in four-point bending for the same strain. This provides a better sensitivity in the measured load-displacement data, which in-turn gives a more accurate thickness measurement. The second important advantage is that the three-point bending geometry is less sensitive to small misalignments. Both aspects will be discussed in the following.

The coupling between mechanical stress and resistivity in a material is described by the rank 4 piezoresistivity tensor. In general, there can be up to 36 independent piezoresistive coefficients in the linear regime. However, if the active material is polycrystalline and therefore isotropic, there will only be two independent piezoresistive coefficients to measure.[6] These two coefficients are typically taken to be the longitudinal π_l and the transverse π_t coefficients and they can be measured when the directions of current and stress are parallel and perpendicular, respectively. In practical measurements of thin-film samples it is, however, often not possible to extract the

[a]ndm@mci.sdu.dk
[b]jkh@mci.sdu.dk

piezoresistivity coefficients because only the applied strain is easily determined from the strain on the surface of the substrate whereas the stress is not. This is due to the compliance tensor often being unknown for thin-film materials which makes it impossible to convert from applied strain to stress. Therefore, rather than piezoresistive coefficients, authors often report gauge factors that relate the resistance change to strain instead of stress. For isotropic materials, two independent gauge factor measurements can be made resulting in a longitudinal and transverse gauge factor. Typically, the longitudinal gauge factor is larger than the transverse gauge factor, and hence, many papers only report the longitudinal gauge factor, which is then labeled "the gauge factor" to a given material.

The overall accuracy of the gauge factor measurement depends on both the accuracy of a mechanical measurement and an electrical measurement performed simultaneously. A high accuracy of the applied strain is much more difficult to obtain than an accurate resistance measurement. Therefore, much attention will be placed on the mechanical side of the gauge factor measurement and the errors associated with the determination of strain.

II. APPARATUS DESIGN

The measurement setup consists of a three-point bending fixture, a commercial mechanical testing apparatus (TA Instruments Q800), and a Keithley 2450 SourceMeter. The electrical connections between the sample and the SourceMeter are achieved through silver contact wires mounted on the fixture supports. An overview of the setup is shown in Fig. 1.

A. Mechanical actuation system

The fixture is installed in a TA Instruments Q800 mechanical testing apparatus. This system features a linear actuator with a force resolution of 0.01 mN and a displacement resolution of 1 nm. The instrument has an air bearing-suspended main shaft, which essentially eliminates friction, thereby, reducing this otherwise important error source to a minimum. We do, however, observe that the instrument has a variation of ±0.1 g during calibration of the clamp mass. The mass of the clamp is 20 g, hence this variation corresponds to a ±0.5% uncertainty on the force measurement. The instrument is equipped with a furnace, which allows measurements to be carried out at temperatures up to 600 °C. The fixture itself has been designed to tolerate temperatures up to 550 °C limited by the insulation material of the cable connecting the silver contact wires to the electronic measurement equipment outside the furnace.

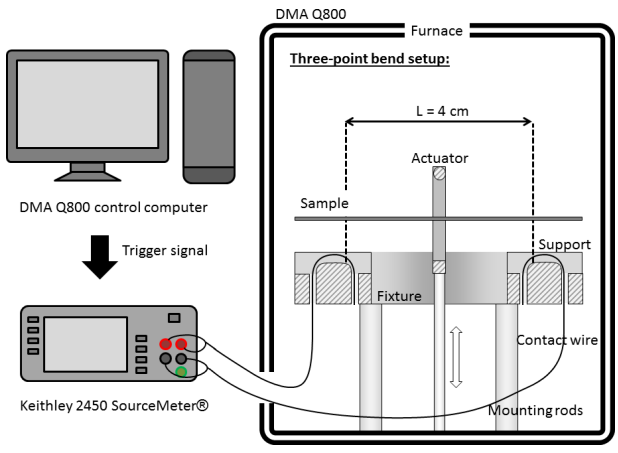

FIG. 1. Overview of the measurement setup. Please see the text for details.

B. Sample

The samples are thin-film resistors deposited onto thermally oxidized silicon wafers. The data shown in subsequent sections have been obtained from a titanium nitride (TiN) thin-film deposited using RF reactive magnetron sputtering from a Ti target and an argon/nitrogen co-flow (6% N_2). The thin-film resistor was patterned into a meander structure with the wires along the long axis of the substrate using photolithography. A 30 nm gold layer was added to the contact pads to insure a good electrical contact. This design enables measurements of the longitudinal gauge factor. The design and orientation of the substrate is shown in Fig. 2. The substrate dimensions are 12.7×58.6 mm^2, hence, six substrates can be made from a four-inch wafer. The length of the substrate matches the length of the fixture which makes alignment quick and accurate. The typical substrate thickness is 0.5 mm, however, the tolerance on the wafer thickness is typically ±25 μm. This tolerance gives rise to a large error when the strain is calculated. The substrate thickness needs to be measured to a accuracy better than 1% to achieve a strain accuracy of 2%. Below we show how the thickness measurement can be integrated into with the gauge factor measurement.

One very important point when using silicon substrates is the anisotropic mechanical properties of the single crystal material. This means that the compliance of the sample depends strongly on the orientation of the sample. This has been thoroughly described by Hopcroft *et al.*[7] For Si (100) wafers with the long axis of the substrate oriented along the [$\bar{1}$10] direction, the equivalent Young's modulus is 169 GPa. For (100) wafers, the flat is typically parallel to the [110] direction to within a precision of ±1°. Such a small variation will give a negligible error on the calculated strain and is, thus not, considered as an error source in the following. However, if the wafer is doped the compliance of the sample can deviate by a few percent from literature values.[8]

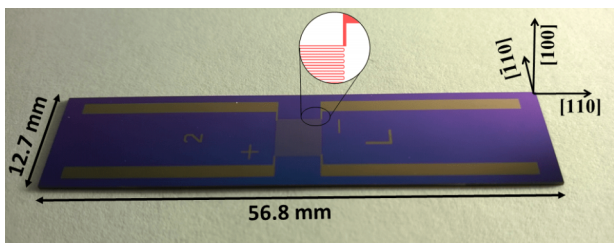

FIG. 2. Longitudinal gauge factor test sample consisting of a Si (100) substrate with a SiO_2 insulation layer onto which a structured TiN film has been deposited. The magnified area shows part of the meander structure layout.

C. Three-point bending fixture

The three-point bending fixture is manufactured from Macor®, which is a machinable ceramic material that is electrically insulating and withstands temperatures of up to 800 °C. In Fig. 3, the fixture design is shown together with the other main components. Referring to Fig. 3: The sample (1) is placed over the support points (2), where two contact wires (5) are suspended over each of the main support blocks. The wires are fixed to the main block through the holes (6) and (7). The load on the sample is applied from the shaft (4), which is connected to a linear actuator and to the clamp (3). The fixture is mounted on four posts (8) in the TA Instruments Q800 mechanical testing apparatus. Four additional wire holes have been added in the design to allow additional contact wires for testing more complex circuits in future applications.

The structural stability of the fixture has been simulated using COMSOL Multiphysics 4.3b. The compliance of the fixture was calculated to be 0.007 μm/N, while the measured compliance was found to be 0.4-0.5 μm/N. The difference is expected to be due to the tolerances in the machining of the fixture and the resulting small misfits between the mounting posts and the fixture itself. The Von Mises stress distribution in the fixture is shown in Fig. 4 for a total load of 10 N. The maximum Von Mises stress in the structure is 1.52 MPa, which is much less than the rated flexural strength of 94 MPa for the Macor ceramic. Moreover, the maximum tensile stress at the critical points near the mounting rods is a factor of 3 lower than the maximum stress. Thus, the fixture is structurally sound over the intended load range of up to 10 N.

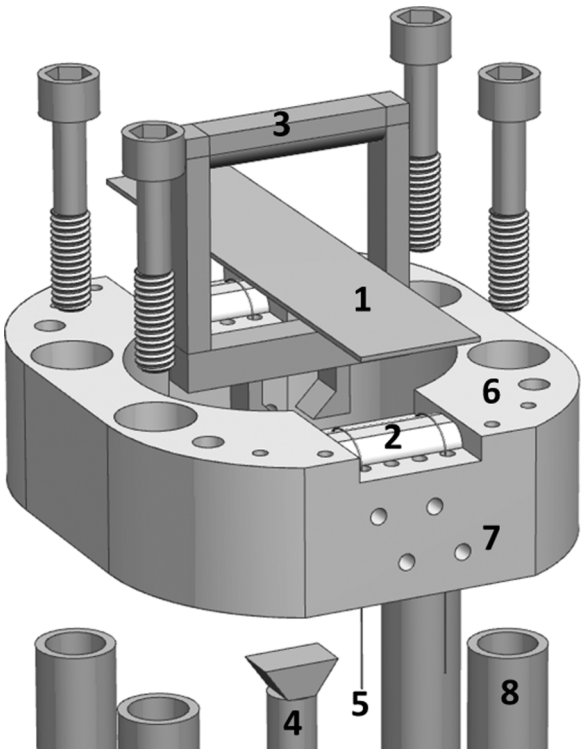

FIG. 3. The custom-made three-point bending fixture, see text for details.

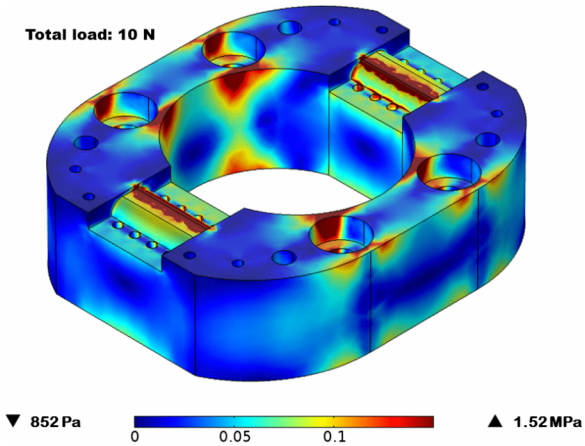

FIG. 4. The Von Mises stress distribution in the fixture. Notice the stress concentrations near the mounting rods.

1. Electrical contacts

The electrical contact to the sample is achieved through the thin wires suspended over the sample supports, see Fig. 3, items (2) and (5). They are kept in place by weaving the wire through the mounting holes, which results in a tight mount. The suspension of the wires over the supports gives the wires a weak spring effect. This insures electrical contact at all four contact points even at low loads (<1 N). The unloaded wires have a 0.1-0.2 mm clearance over the support block. Once the sample is loaded, the wires will rest on the edge of the fixture block. The contact resistance has been estimated to be less than 0.5 Ω and it decreases by 0.2 Ω when loaded to 2 N. The wires are made from 99.99% silver and have a diameter of 0.10 mm.

Silver was chosen for its high conductivity and low hardness. The low hardness causes the wire to plastically deform at a relatively low load and it thereby protects the sample from high concentrated stresses at the contact points, which would otherwise arise. The elastic stress in a point of contact between two elastic bodies can be calculated using contact mechanics.[9] The curvature of the silver wire at the point of contact to the sample is 0.05 mm in the direction perpendicular to its length and 2.1 mm along the length of the wire, i.e., curvature of the support. The load needed to initiate plastic deformation in the silver wires has been estimated using the Hertz theory. The Young's moduli of silver and of a silicon(100) surface are 77 GPa[10] and 130 GPa,[7] respectively. If we assume that the plastic deformation occurs when the average contact pressure is equal to the hardness of silver, which is 400 MPa,[11] then the total load needed to initiate plastic deformation is less than 5 mN. Thus, the wire will start to conform to the Si substrate as soon as the wire is pressed into contact with the support. In contrast, the Si substrate and the SiO_2 insulation layer have hardnesses of 10 GPa and 9 GPa, respectively.[12,13] The large difference in the hardness between the sample and the silver wire insures that the sample is not damaged during loading since the mean contact pressure cannot be higher than the hardness of the silver wire. In Fig. 5(a), the plastic deformation of the silver wire is shown after the sample had been loaded to 10 N. Due to the deflection of the sample during loading, the pressure of the sample on the wire

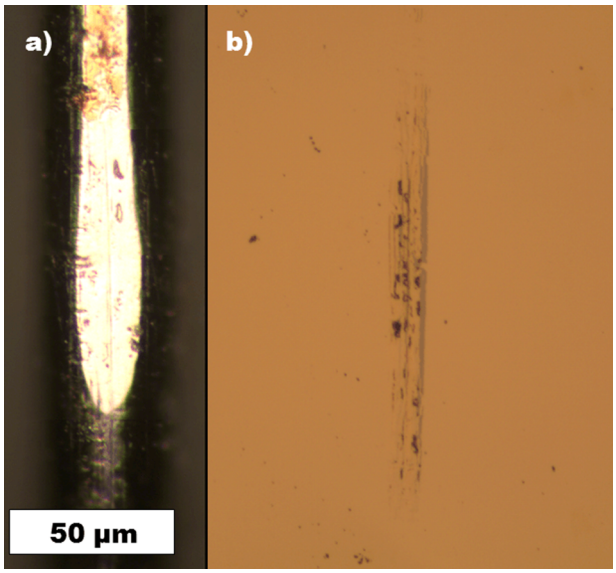

FIG. 5. (a) The deformed silver wire at the contact point. The contact point shifts downwards as a function of the load due to the rounded support edge. Higher loads give larger deformations. Some of the soft gold from the samples has transferred to the wire. (b) Au contact layer on the TiN film after contact with the silver contact wire.

becomes concentrated on the chamfered edge as the loading is increased. Thus, the plastic deformation becomes more severe as the loading is increased and the contact point shifts. The deformation insures a good contact to the sample and also prevents excessive stresses in the substrate. Furthermore, the deformation of the silver wires will help compensate possible deviations in the fixture support flatness that may be present due to machining tolerances, i.e., a slightly protruding wire will have to carry more load and hence will deform more whereby the error is minimized. In Fig. 5(b), the TiN sample is shown after being tested in the setup. The soft gold is slightly damaged by the wires during measurement and gets partly transferred to the wires. Naturally, the insulating SiO_2 layer has to be of high quality to prevent electrical connection to the substrate. However, during tests of over 100 samples, many which have been tested repeatedly (some more than 10 times), no problems with electrical leakage to the substrate were observed.

III. MEASUREMENT PROCEDURE

The measurement procedure consists of three steps, (1) mounting and aligning the sample on the fixture, (2) running the measurement protocol, and finally (3) data analysis. The alignment of the sample is very simple: the ends of the sample have to coincide with the ends of the fixture. It is estimated that the alignment error in the direction along the long axis of the substrate is less than 0.5 mm. After the sample has been mounted on the fixture, the test procedure initiates with three loading cycles followed by the test sequence itself. In Fig. 6, the loading sequence is shown as applied load versus time for a single gauge factor measurement. The first three full loading cycles insure that any plastic deformation in the wires has progressed before the test measurement sequence itself

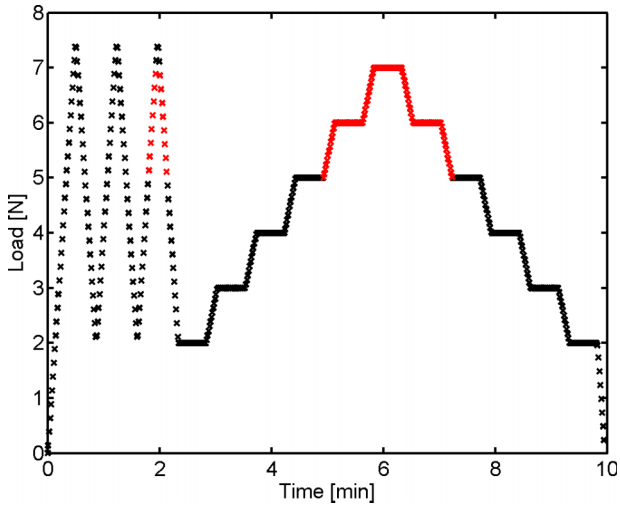

FIG. 6. The loading sequence used in gauge factor tests. The red points are the points used for fitting the slope in the load-displacement data, see below.

initiates. This is especially important when a new set of contact wires has been installed and is only done once when characterizing the same sample at multiple temperatures. Typically, the load-displacement curve has a low hysteresis and a high reproducibility. In this case, the sample is correctly mounted. If the sample is misaligned and is contacting the vertical sides of the fixture, it is readily seen in the load-displacement curve as a large friction-induced hysteresis effect. High levels of friction in the load-displacement data will compromise the repeatability and accuracy of the measurement as discussed in further detail below. If a friction-induced hysteresis is observed, the sample needs to be re-aligned.

A. Electrical measurements

The Keithley 2450 SourceMeter is programmed to measure a current-voltage (I-V) curve at each step in the loading sequence and the resistance is extracted as the slope of the I-V curve. The electrical measurements are initiated during the three initial loading cycles described above starting with a single resistance measurement to set the current sweep range and voltage measurement range of the SourceMeter. If the ranges are controlled by the automatic function of the instrument, it might change ranges during the loading sequence, which can result in a small offset shift in the measured I-V curves where the instrument range was shifted. The relative resistance changes observed in low-gauge factor materials are of the order of 10^{-4} at elastic strain levels. Such low resistivity changes make direct observation of the resistance change from the slopes of the I-V curves difficult, see Fig. 7 (inset a). In Fig. 7 (inset b), the resistance is shown as a function of the applied load. The expected linear relationship allows us to extract the unstrained resistance of the sample, denoted R_0. In the main panel of Fig. 7, the I-V curves at different loads are shown with the unloaded I-V curve subtracted. This demonstrates the change in the slope of the I-V curves at different loads, which directly gives the change in resistance. The low hysteresis in the measurement is also directly visible in this plot as the I-V curves during loading and unloading nearly

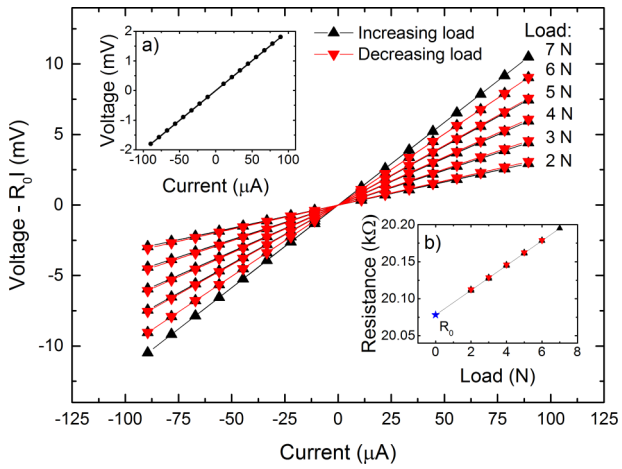

FIG. 7. *(Inset a)*: The I-V curves made at different loads. All curves essentially coincide in this plot. *(Inset b)* The resistance versus load. The unloaded resistance is extrapolated from the data. *Main panel*: The I-V curves plotted with the unloaded I-V curve subtracted.

coincide. The main advantage of measuring the resistance as the slope of a I-V curve rather than a point measurement at a single current is that it eliminates voltage offsets in the instrumentation or offset induces by thermoelectric effects when the test is performed at elevated temperatures. Moreover, thermoelectrical effects are directly visible as a voltage offset at zero current, see also below. Furthermore, the plots in Fig. 7 also give a good representation of the quality of the measurement data and reveal nonlinearities due to, for example, resistive heating of the sample.

IV. DATA ANALYSIS

The data analysis is mainly made on the mechanical data to extract the correct strain in the resistor area. The electrical data do not require any further analysis than what was shown in Sec. III. The strain analysis is made using the Euler-Bernoulli beam theory. This approach has subsequently been validated using finite-element modeling (FEM).

A. Beam theory

In the Euler-Bernoulli beam theory, the deflection, δ, of a rectangular sample, which is simply supported and centrally loaded, is given by[14]

$$\delta(x) = \frac{Px}{4Ebh^3}\left(3l^2 - 4x^2\right), \quad 0 < x < l/2, \tag{1}$$

where P is the applied load, E is the appropriate bending modulus as discussed in Section II B, l is the suspension length, b is the beam width, h is the beam thickness, and x is the distance measured from the support to the point where the deflection is evaluated, see the x-axis in Fig. 10. It is noted that the deflection at any point of the beam is linearly proportional to the applied load and the constant of proportionality is determined by the geometry and the bending modulus of the beam. In fact, this relation is used in standard methods of determining elastic moduli of certain types of materials.[15] The longitudinal strain, ϵ_{xx}, at the surface of the beam is given by[14]

$$\epsilon_{xx} = -\frac{h}{2}\frac{d^2\delta}{dx^2} = \frac{3P}{Ebh^2}x, \quad 0 < x < l/2. \tag{2}$$

Thus, it is seen that the strain varies linearly from zero at the supports to the maximum value at the center of the beam. The deflection and strain are symmetric about the loading point. The non-constant strain over the active gauge area has often been quoted as a disadvantage of three-point bending in comparison to the constant strain obtained in a four-point bending setup. However, when the piezo-resistive response of the material is linear this problem is easily overcome. If we consider a resistor of constant width parallel to the x-axis on the surface of the beam under load, then the resistance of a small part of the resistor, dl, is given by

$$dR = \frac{\rho}{A}dl, \tag{3}$$

where ρ is the resistivity of the resistor material and A is the cross-sectional area. If the resistor is subject to strain, the resistance of the small part of the resistor can be described as

$$dR = \left[\frac{\rho}{A} + \left(\frac{1}{A}\frac{d\rho}{d\epsilon_{xx}} + (1+2\nu)\frac{\rho}{A}\right)\epsilon_{xx}\right]dl, \tag{4}$$

where $\frac{1}{A}\frac{d\rho}{d\epsilon_{xx}}$ is the intrinsic piezoresistive response and $1+2\nu$ is the geometrical term.[16] It should be noted that the geometrical term presented here does not take into account that the resistor is bonded to the substrate. This situation has been evaluated by Dössel.[17] Taking the integral of the resistance along the length of the resistor and assuming that the piezoresistive response is linear yields

$$R = \int_0^{l_0}\left[\frac{\rho}{A} + \left(\frac{1}{A}\frac{d\rho}{d\epsilon_{xx}} + (1+2\nu)\frac{\rho}{A}\right)\epsilon_{xx}\right]dl \tag{5}$$

$$= R_0 + \left(\frac{l_0}{A}\frac{d\rho}{d\epsilon_{xx}} + (1+2\nu)\frac{\rho l_0}{A}\right)\langle\epsilon_{xx}\rangle \tag{6}$$

$$= R_0 + R_0 G_L \langle\epsilon_{xx}\rangle, \tag{7}$$

where $\langle\epsilon_{xx}\rangle$ is the average strain along the resistor and G_L is the longitudinal gauge factor of the resistor. Thus, the longitudinal gauge factor of the resistor can be evaluated in the usual way by taking the strain to be the average strain over the active area of the resistor. A similar argument can be made for a transverse gauge factor measurement. This method is valid as long as the gauge factor is well defined, i.e., when the resistance change is linearly proportional to the applied strain. The average strain on a resistor area with length χ along the x-axis of the substrate is given as

$$\langle\epsilon_{xx}\rangle = (L - \chi/2)/L \cdot \epsilon_{xx,max}, \tag{8}$$

where $\epsilon_{xx,max}$ is the strain at the center of the beam.

1. Wafer thickness

The thickness of the substrate is critical in the calculation of the surface strain since it enters the equation for the strain to the second power. Furthermore, it is also the geometrical parameter in Equation (2), which is most difficult to measure accurately. For example, profilometers have very high accuracies and resolution, however, the sample must be placed on

a completely flat and particle free surface to avoid overestimating the sample thickness. We found that the most precise way to measure the wafer thickness is to simply weigh the samples and exploit that the samples are diced into precise dimensions and the well-defined density of a single-crystalline material.

Instead of using a direct thickness measurement, it is possible to extract the thickness of the sample directly from the measured load-displacement data. The slope of the load-displacement curve can be used to calculate the thickness of the sample, since the slope is related to the thickness of the sample as

$$\frac{dP}{d\delta} = \frac{4Ebh^3}{l^3}. \tag{9}$$

In Fig. 8, the load-displacement curve of a silicon sample loaded up to 7.5 N is shown. During the initial of the loading, up to 2 N, the sample is pressed against the wire contacts until these rest on the support. Hereafter the load-displacement curve becomes linear as expected from Equation (1). The slope is taken from a fit to the load-displace curve from 7 N to 5 N. In Fig. 8 the data points used for the linear fit correspond to those indicated in red in Fig. 6. It is observed that the fit follows the measured data also at the lower loads. For comparison, lines corresponding to ±10 μm substrate thickness variation have been plotted in the figure. The uncertainty of the thickness measurement is calculated from the standard deviation of the fitted slope. This error is typically 0.2% or less.

The reproducibility of the measured thicknesses is ±2 μm. Larger deviations can occur if the sample touches the sides of the clamp. However, in this situation, the resulting load-displacement data will have a non-smooth load profile and large hysteresis. Thus, this error is easily detected and the sample can be repositioned in the fixture.

In Fig. 9, the measured thicknesses of 36 samples are plotted against their thicknesses as determined from their mass. The linear fit to the data set shows that the slope is 0.6% less than unity, indicating that the thickness measured with the three-point bending setup is slightly less than the result from the weight measurement. The mean deviation in the thickness

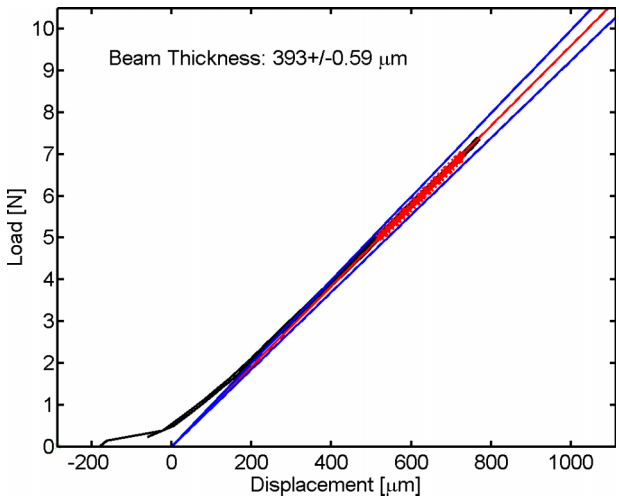

FIG. 8. The load-displacement curve of a silicon substrate. The blue lines are slopes corresponding to ±10 μm substrate thickness.

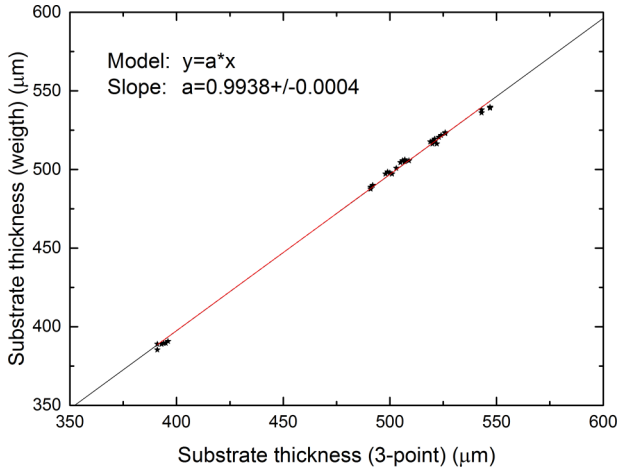

FIG. 9. Thickness measurements of 36 samples with the 3-point bending setup and by the weighting method. A few points overlap and cannot be distinguished.

data is 0.65%. The integrated thickness measurement implemented in this setup can also provide a consistency check of the measured data against an independent measurement of the substrate thickness. Thus, if significant error sources are present in the experiment, e.g., an unexpected crystallographic orientation of the substrate, this would immediately be visible as a discrepancy in the measured thicknesses. Alternatively, the analysis can be rearranged to test the modulus of the substrate allowing the test of strain gauges deposited onto substrates with unknown modulus.

B. FEM strain distribution

The strain found using the beam theory is an approximate solution of the strain distribution in the sample under load. A more accurate solution has been obtained through a finite element simulation performed in COMSOL Multiphysics 4.3b. The sample used in the simulation had a thickness of 500 μm and the anisotropic compliance tensor was used in the constitutive equations. In Fig. 10(b), the longitudinal strain distribution, ϵ_{xx} on the tensile side of the sample is shown. The resistor area is marked by a square. The strain along the dashed line is plotted in Fig. 10(a) together with the analytical Euler-Bernoulli solution. There is a close resemblance between the simulation result and the analytical solution. The largest deviation is found at $x = l/2$ where the simulation gives a strain 1.4% higher than the analytical solution. However, it is the average stain over the resistor area, which is used in the calculation of the gauge factor. The deviation in the average strain over the resistor area is only 0.17%. The transverse strains, ϵ_{yy} are less than 1% of $\epsilon_{xx,max}$ over the resistor area. This is due to the very weak coupling between perpendicular strains in silicon (100) wafers with the x-axis oriented along the [110] direction. Between these directions, the Poisson ratio is as low as $\nu = 0.064$.[7] Thus, in the gauge factor measurement, it is not necessary to consider the contribution of transverse strains to obtain a pure longitudinal gauge factor when silicon (100) wafers are used.

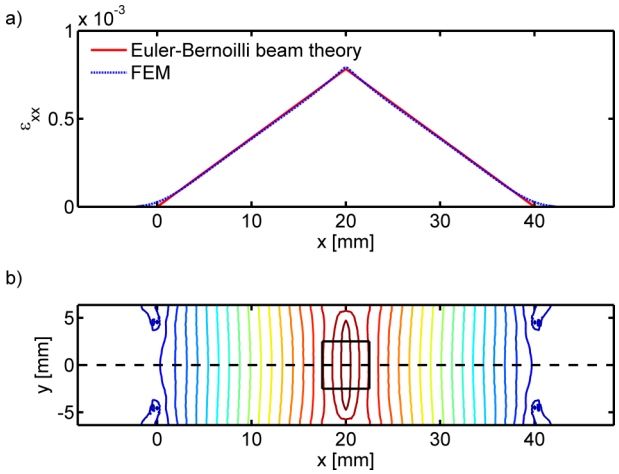

FIG. 10. (a) The longitudinal strain, ϵ_{xx} at 7 N load. The values are taken along the center of the sample as indicated by the dashed line in (b). The strain calculated by Equation (2) is also represented in the plot. (b) The contour map of the strain.

C. The gauge factor

Once the resistance and strain have been determined as a function of the applied load, it is a simple matter to find the gauge factor. In Fig. 11, the relative change in resistance is plotted against the applied average strain, the slope corresponds to the gauge factor. The deviation on the gauge factor value shown in the figure is the statistical standard deviation derived from the least squares fit to the data points.

The maximum strain corresponds to 190 MPa, which is much less than the yield stress of silicon that has been measured by Petersen to be 7 GPa.[18]

V. ERROR ESTIMATES

A low sensitivity of the loading geometry to small misalignments is important to achieve robust and accurate measurements. The setup is constructed to utilize the high precision actuator of the TA Instruments Q800 DMA. The electrical measurements are precise to 5 digits. Thus, the accuracy of the measured resistance, load, and displacements are high (>0.5%). The primary source of error, therefore, comes from misalignments and machining tolerances. In Sec. V, the sensitivity of the setup to the most important of the possible misalignments is discussed.

A. Longitudinal position and loading point offset

The most obvious source of error in the three-point setup is a misalignment along the x-axis. In this case, the maximum strain will not occur at the center of the active resistor area. This problem has often been the primary argument for choosing a four-point bending setup since a constant strain can be achieved between the inner load points in this geometry. The strain at the center of the resistor area is very sensitive to this alignment error, however, it is important to note that in the gauge factor calculation, the average strain is used. Thus, it is the error in the average strain that is important for the accuracy of the measurement. In Fig. 12, the errors associated with both the strain at the center of the resistor area and the average strain are shown. It is clear that the strain at the center of the resistor area is very sensitive to the placement of the sample. On the other hand, the relative error of the average strain is much lower. If the sample placement is made with an accuracy of ±0.5 mm, the error will be less than 0.3%. If a deviation of ±1 mm is assumed, the error is within ±1%. The sensitivity of the average strain error is very dependent on the size of the active area. In the zero area limit, the error is the same as that for the center strain. In Fig. 12, the error due to eccentric loading is also shown, i.e., an offset in the loading point along the x-axis. This error is insignificant for the three-point setup. In contrast, this type of misalignment in the four-point setups can lead to significant errors (an order of magnitude higher than in three-point setups).[19]

B. Tangency point shift

The radius of the supports will cause the actual support points to shift with higher deflection due to the change in the

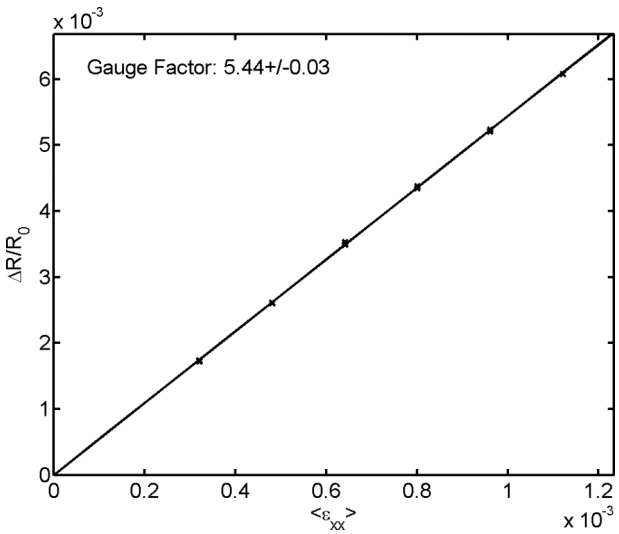

FIG. 11. The resistance change plotted against the applied strain. The gauge factor is given by the slope of the line fitted to the data.

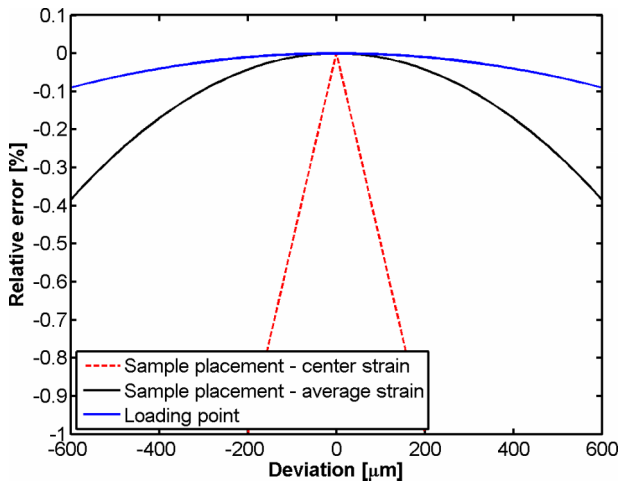

FIG. 12. The mis-alignment error due to sample placement along the x-axis for the center strain and average strain. The error due to a misalignment of the load point is also shown.

angle between the beam and the support. This will impact the suspension length of the beam. This can be inferred from Fig. 5(a), where the deformation of the wire is the result of the support point of the sample shifting with higher loads. It should be noted that shape of the supports corresponds to two quarter circles with a flat plateau joining them, thus, the wire is deformed across the plateau at low loads before resting on the edge at higher loads. This design was chosen to insure the spring effect giving good contact also at low loads. Therefore, there is a stronger effect of the tangency point shift at low loads. However, the choice of the starting load of 2 N in the gauge factor measurement minimizes the influence of this effect. The effect of the tangency point shift has been analyzed by Quinn *et al.*[20] for three- and four-point bending setups. If we take the radius of the supports to be 2 mm and the sample thickness to be 0.5 mm, the error is 0.8% for three-point bending while it would be 1.7% for four-point bending.

C. Friction

Friction at the support-contact point can potentially result in large errors in the applied strain. The friction at the support points will create a bending moment, which counteracts the moments created by the vertical forces acting on the beam. This will systematically reduce the strain present in the beam leading to an overestimation of the strain in the beam during loading. This error can be calculated from

$$error = \left(\frac{\epsilon}{\epsilon_0}\right) = 100\% \cdot \left(\frac{\mu}{L/2h - \mu}\right), \tag{10}$$

where μ is the friction coefficient between the sample and the support, see Refs. 19 and 20 and references herein. The friction coefficient of metal-to-metal contacts is typically in the range 0.3–1. For the typical sample thickness of 0.5 mm, the error on the applied strain due to friction has an upper bound of 2.56% in the present system. FEM was also employed to further elucidate the effect of friction on the measurement results. A friction traction force, $\mu P/4$, was added at the support points in the model. The error under the same conditions as used in the estimate above resulted in an error of 1.64%. The deviation on the load-displacement slope was also calculated from the FEM results. It was found that the displacement would be 1.87% less than in no friction case. Given the irreversible nature of frictional forces, the presence of friction in the setup will result in hysteresis in the load-displacement curve. A small hysteresis in the slope of the load-displacement curve between loading and unloading has been observed in the range of 1%-2%. This is comparable to the difference in the slope found in the FEM result and thus gives an upper bound of the error due to friction of ~2%. The irreversible nature of frictional forces means that in the loading case the deflection is expected to be less than in the friction-free case and vice-versa for the unloading case. Thus, when the slope is fitted to both the loading and unloading curves and the effect of friction acts in opposite directions in these two cases, thus, the error on the fitted slope of the load-displacement curve should be significantly less than the worst-case estimates given above.

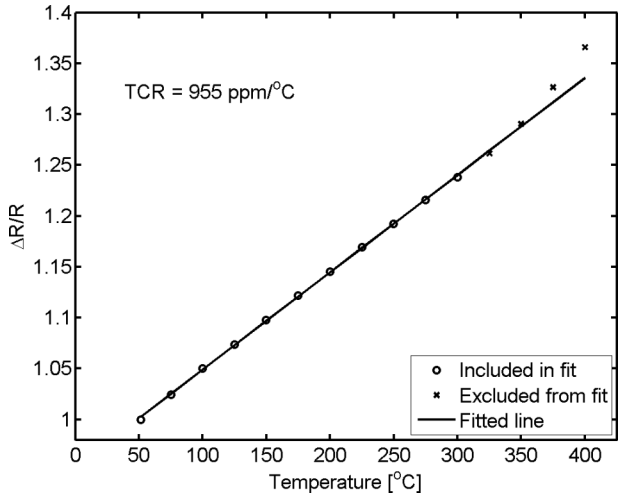

FIG. 13. The unloaded resistance relative to the room temperature resistance plotted against temperature. The TCR is the slope of the linear fit.

VI. MEASUREMENTS AT ELEVATED TEMPERATURES

The setup has been designed to characterize samples up to 550 °C. In the following, we present the results of a test of a TiN sample tested up to 400 °C.

A. Temperature coefficient of resistivity (TCR)

The TCR value of the sample is readily extracted from the measurement data. The resistivity of the unstrained sample, R_0, is extracted after each load cycle as seen in Fig. 7(b). In Fig. 13, the resistance change normalized at 50 °C is plotted against temperature. The slope of this plot is the temperature coefficient of resistivity (TCR). We note that the measurement points start to deviate from the linear behavior at the highest temperatures. The TCR value of this particular sample is 955 ppm/°C. The positive value indicates a metallic conduction mechanism in the sample.

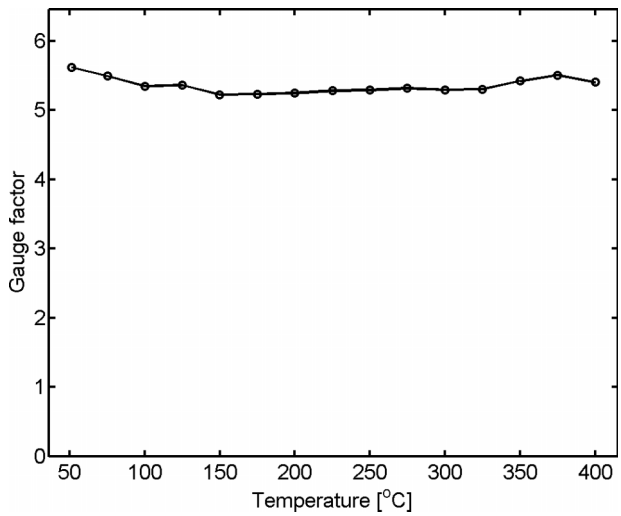

FIG. 14. The gauge factor as a function of temperature.

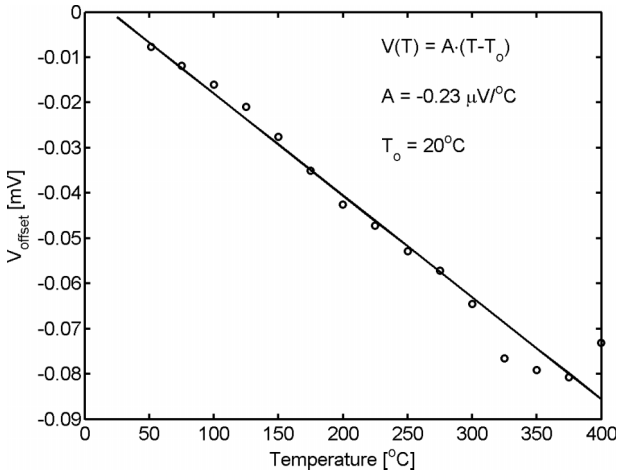

FIG. 15. The offset voltage at zero current as a function of temperature. The slope, A, corresponds to the relative Seebeck coefficient of the system. T_o is the temperature at terminals in the SourceMeter.

B. Gauge factor versus temperature

In Fig. 14 the gauge factor versus temperature is shown. The gauge factor for the sample is fairly stable over the temperature range. The sample has not been exposed to 400 °C before the test, thus, some resistivity drift effects are present in the data at higher temperatures. However, the effect of a constant drift rate cancels out in the fit of the gauge factor because both the load and unload data are used for the fit, hence a constant drift rate does not impact the gauge factor measurement. Rather, the fairly high TCR values of the sample give some non-linear drift in the measurement data during the resistance measurement cycle due to half a degree of temperature variation. Despite this, the variation in the measured gauge factor is less than ±4% over the measured temperature range.

C. Thermoelectrical effects

As mentioned in Section III A, thermoelectrical effects are compensated by measuring the resistance as the slope of an I-V curve, rather than a simple ratio. In the discussion in relation to Fig. 7, it was mentioned that any thermoelectrical effect would be seen as an offset voltage of the crossing point of the I-V curves occurring at zero current. This offset voltage has been plotted versus temperature in Fig. 15. The relative Seebeck coefficient extracted from this setup is low, −0.24 μV/°C, compared to typical values for thermocouples. Still the effect would be the source of large errors in the resistance measurements at low current levels if a simple resistance measurement is made without taking the thermoelectrical effects into account.

VII. SUMMARY AND FINAL REMARKS

We have presented a method and a setup for measuring piezoresistive gauge factors using three-point bending. The setup allows testing up to 550 °C and the results of a test of a sample heated up to 400 °C were presented. The electrical resistance was extracted from I-V curves thereby eliminating thermoelectrical effects. The bending deflection data were used to determine the thickness of the Si sample thereby eliminating an additional measurement. The strain in the sample was calculated using the Euler-Bernoulli beam theory and compared to results from FEM simulations. The most important error sources were evaluated and compared to four-point bending. We estimate that the combined errors lead to an uncertainty in the gauge factor measurement of 2%-3%.

ACKNOWLEDGMENTS

The authors would like to thank Reiner Hübel for skillful machining the Macor piece and Kasper Thilsing-Hansen for many inputs in the early design phase. The authors would also like to thank Innovation Fund Denmark (the former Advanced Technology Foundation) for financial support under Grant No. 127-2013-5.

[1]P. Kayser, J. Godefroy, and L. Leca, Sens. Actuators, A **37-38**, 328 (1993).
[2]J. D. Wrbanek, G. C. Fralick, J. M. Gonzalez, and K. L. Laster, NASA/TM 215256 (2008), available at https://ntrs.nasa.gov/search.jsp?R=20080025999.
[3]J. Richter, "Piezoresistivity in microsystems," Ph.D. thesis, DTU Nanotech - Technical University of Denmark, 2008.
[4]E. Lund and T. G. Finstad, Rev. Sci. Instrum. **75**, 4960 (2004).
[5]J. Richter, M. B. Arnoldus, O. Hansen, and E. V. Thomsen, Rev. Sci. Instrum. **79**, 044703 (2008).
[6]R. E. Newnham, *Properties of Materials: Anisotropy, Symmetry, Structure* (Oxford University Press, 2005).
[7]M. A. Hopcroft, W. D. Nix, and T. W. Kenny, J. Microelectromech. Syst. **19**, 229 (2010).
[8]J. J. Hall, Phys. Rev. **161**, 756 (1967).
[9]K. L. Johnson, *Contact Mechanics*, 9th ed. (Cambridge University Press, 1985), pp. 95–99.
[10]M. Sugano, K. Osamura, and A. Nyilas, Phys. C **412-414**, 1114–1119 (2004).
[11]Q. Ma and D. R. Clarke, J. Mater. Res. **10**, 853 (1995).
[12]L. J. Vandeperre, F. Giuliani, S. J. Lloyd, and W. J. Clegg, Acta Mater. **55**, 6307 (2007).
[13]H. Li and J. J. Vlassak, J. Mater. Res. **24**, 1114 (2009).
[14]E. Oberg, F. D. Jones, H. L. Horton, and H. H. Ryffel, *Machinery's Handbook*, 28th ed. (Industrial Press, New York, 2008), p. 258.
[15]"ASTM D790 - Standard test methods for flexural properties of unreinforced and reinforced plastics and electrical insulating materials," 2015.
[16]T. M. Adams and R. A. Layton, *Introductory MEMS*, edited by Adams2010 (Springer, Boston, MA, US, 2010).
[17]O. Dössel, Sens. Actuators **6**, 169 (1984).
[18]K. E. Petersen, Proc. IEEE **70**, 420 (1982).
[19]F. I. Barratta, W. T. Matthews, and G. D. Quinn, "Errors associated with flexure testing of brittle materials," Technical Report MTL TR 87-35 (U.S. Army Materials Technology Laboratory, Watertown, MA, 1987).
[20]G. D. Quinn, B. T. Sparenberg, P. Koshy, L. K. Ives, S. Jahanmir, and D. D. Arola, J. Test. Eval. **37**, 101649 (2009).